Autonomous Close Proximity Differential Drag Control of Satellite Formations using an Inter-Satellite Radio Frequency Link

Melrose Brown, Edwin G. W. Peters, Matthew Dilkes, Ryan Jeffreson, Andrew Lambert, Rabbia Saleem, Russell Boyce, Ed Kruzins, Timothy Bateman
UNSW Canberra Space, University of New South Wales, Australia

ABSTRACT

Close proximity satellite formation flying in Low Earth Orbit (LEO) offers the potential to disaggregate complex missions from large single satellite platforms, to constellations of small satellites that can offer greater resilience and redundancy for the same cost. Close-proximity formation flying is traditionally achieved through closed loop control of active onboard propulsion systems. One solution to avoid the complexity and risk of integrating onboard propulsion is to use differential aerodynamic drag to control the relative motion of the spacecraft without the need for an active propulsion system. The approach involves a drag plate on each satellite that is tilted with respect to the direction of the satellites' velocity to change the drag force experienced by the spacecraft relative to one another, creating the ability to affect the along-track spacing of the satellite formation.

Real-world applications of differential aerodynamic drag typically use deployed solar panels as drag plates. The spacecraft attitude determination and control system (ADCS) controls the orientation of the solar arrays relative to the velocity direction. An operational example of this approach is found in the Planet Flock constellation. To date, differential drag has been used by satellite operators for coarse control of the spacing between constellation members at large along track distances. Theoretical concepts for the use of differential aerodynamic drag control for close proximity operations have been reported in the literature; however, no on-orbit demonstrations were performed prior to the Australian 'M2' 6U CubeSat pair in April 2022, owned and operated by the University of New South Wales (UNSW), Canberra. Using an open 'human in the loop' control approach, UNSW Canberra Space successfully reduced the along-track separation of M2-A and M2-B from 160 km to hold a steady along-track separation distance of 2 km from 11-14 April 2022.

The work presented here analyses different concepts for removing the time-intensive human-in-the-loop control approach and replacing it with a simple, autonomous, closed-loop control system suitable for real-world close-proximity station keeping on the M2 spacecraft. The paper reports on the results from an inter-satellite radio frequency (RF) link experiment conducted on the spacecraft in Q4 2022 and uses the results to inform the performance characteristics of a simulated inter-satellite RF ranging capability using the M2 spacecraft UHF transceivers. The performance of the autonomous, on-orbit, control approach is compared with potential improvements for ground-station-based formation control.

The work begins with an analysis of the autonomous control system on orbit while operating under ideal conditions, where 100% of the orbit is available for differential drag manoeuvres, before exploring off-nominal conditions caused by the temporary loss of attitude control from system resets. Two modes of operation are investigated: a station keeping mode, with the sole aim to minimise the change in relative along track position; and an along track target mode, where the controller seeks to change the along track separation distance to meet a specified value. The effect of uncertainty in the RF-based range measurements for relative orbit control is investigated through simulations and the maximum range of the intersatellite RF ranging sensor estimated from the on-orbit experiments conducted in Q4 2022. Recommendations are provided for the use of the control methodology to support the objective of the M2 maritime optical and RF surveillance mission.

1. INTRODUCTION

1.1 Background

Small satellites are constrained by size, weight, and power (SWaP), requiring careful trade-offs and optimisation of resources to support their main mission payloads. Propulsion systems add complexity in the engineering, testing, and

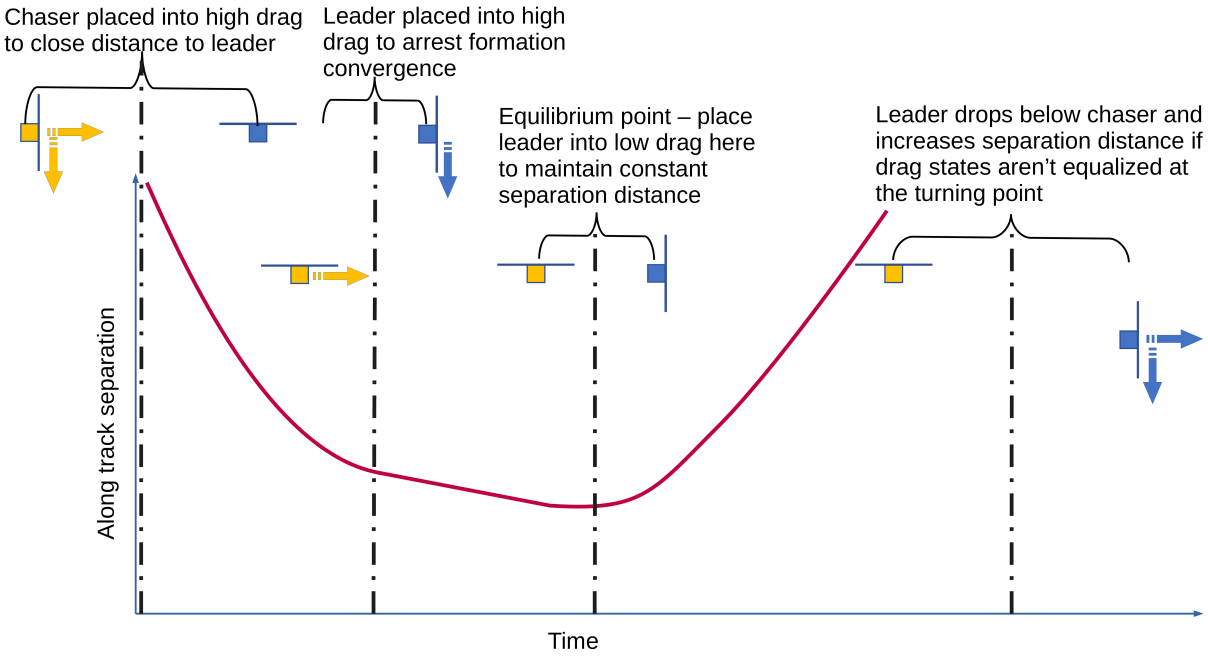

Fig. 1: Differential aerodynamic formation control concept, taken from [cite]

qualification of the spacecraft and are often omitted from CubeSatellite buses. However, formation control between two coplanar spacecraft can still be performed through the action of differential aerodynamic drag [1][2][3][4][5]. Many approaches in the literature propose the use of the attitude control system of the spacecraft to change the effective drag area of the spacecraft, allowing the spacecraft rate of decay due to atmospheric drag to be controlled between the spacecraft (Fig. 1).

Theoretical differential autonomous aerodynamic control concepts within the literature typically assume an accurate determination of each spacecraft's current state vector, an accurate knowledge of the current and future atmospheric density, and the ability to communicate and control each spacecraft throughout the orbit. Communication is required between the spacecraft, and often assumed to occur via either an intersatellite communication system or low-latency communication to a ground segment to optimise changes in each satellite's attitude to perform a given manoeuvre target, which can introduce additional complexity to the overall mission architecture. The operational implementation of differential aerodynamic drag is limited to control at large ranges [6] where only coarse control is required.

The application of differential aerodynamic drag for close proximity formation flying manoeuvres is sparse, with the UNSW Canberra 'M2' satellite formation [7] representing the first known on-orbit demonstration of differential aerodynamic control for formation control under 5km in range. Close proximity formation flying for the M2 mission supports the space, maritime, and Earth observation payloads and associated domain awareness primary mission objectives. The ability to control the spacing of the spacecraft creates opportunities for tipping and cueing between the RF and optical sensors, creating a baseline for time and frequency difference of arrival passive RF sensing, and interferometry [8]. The M2 formation additionally serves as a validation and verification target for improving ground-based space domain awareness sensors and mission systems for Low Earth Orbit close proximity operations [7].

The M2 mission was launched on 22nd March 2021 into a nominal 550km, 45° inclination orbit and initially deployed as a conjoined 12U satellite. The spacecraft were commanded to separate on 9th September 2021, where they split into 2x6U CubeSats, M2-A (satno 47967) and M2-B (satno 47973) via the action of a small spring between the spacecraft. Each spacecraft deployed multiple solar arrays and antennae (Fig. 2), creating a large attitude-dependent area-to-mass ratio, which is exploited for differential aerodynamic control.

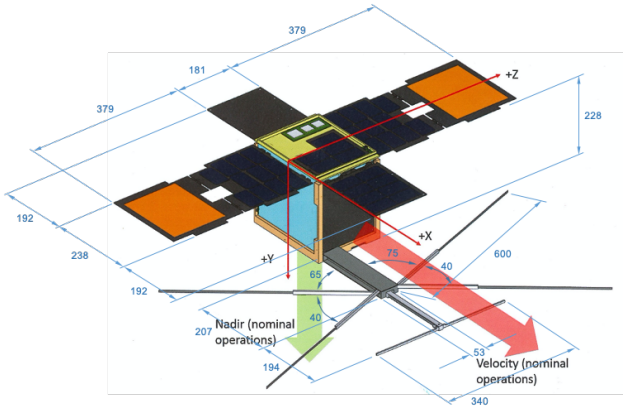

Fig. 2: Dimensions for a deployed M2 satellite configuration

2. METHODOLOGY

2.1 Challenges for Differential Aerodynamic Drag Formation Flying with the 'M2' Spacecraft

The M2 formation has been controlled using a human-in-the-loop approach since the spacecraft divorced from a 12U CubeSat into a formation of two (non-standard) 6U platforms. To date, the approach has involved downlinking sufficient GPS data from each spacecraft for accurate Orbit Determination (OD) and derivation of each spacecraft's drag/ballistic coefficient from the state estimation process. The OD is performed using the batch least squares estimator within NASA's General Mission Analysis Tool (GMAT)[9]. A 40^{th} degree and order EGM96 gravity model is applied. Atmospheric drag is modelled using a spherical drag model and the MSISE90 atmosphere model, using the CSSIS Space Weather File updated daily from Celestrak [10]. Future atmospheric density is derived from the predicted Kp and ap indices contained in the CSSIS Space Weather files. Third-body accelerations from the Moon and Sun are modelled as point masses. Solar radiation pressure and Earth tides are ignored.

The manufacturer provided test results with the Spirent GSS7000 GPS simulator, demonstrating a mean position error of 1.2378 m and a maximum error of 3.2714 m for the Venus838 GPS receiver used onboard the spacecraft. A conservative noise sigma value of 10m is applied in the GMAT batch estimation during the OD process. The batch estimator is initialised using the first GPS data point in the data series and a drag coefficient C_d = 1.5 over a nominal area of $0.07m^2$. The estimator solves for Cartesian state and C_d.

The change in relative motion in the along-track direction is achieved through changing the satellite's attitude to present either a "low drag" or "high drag" area towards the velocity direction. Holding the nominal spacecraft area constant in the GMAT simulation, the resulting change in high and low drag manifests itself as a change in the estimated C_d. It is important to note that the estimated value for $C_d{}^{high}$ and $C_d{}^{low}$ change over time, primarily due to mis-modelling of the atmosphere; the pointing accuracy of the spacecraft (estimated to be up to $\pm 15^{\circ}$); short periods each day when the spacecraft have to break from their nominal pointing task to perform ground station pointing for data downlink or brief periods where the spacecraft; the amount of GPS data available; and reductions in the theoretical maximum and minimum drag pointing attitudes to improve power generation through secondary axis pointing solar arrays towards the Sun. Figure 3 shows the change in C_d estimates over time for the M2-A and M2-B spacecraft in both high- and low-drag configurations.

The OD assumes a constant C_d over the estimation window and therefore requires a GPS data stream without any manoeuvres, i.e. the spacecraft must be tasked with the same nominal high or low drag pointing throughout the entirety of the dataset used to perform the OD estimation. Typically, 1-2 days of GPS data is required to provide a state estimate of sufficient accuracy to predict and model formation manoeuvres. The effect of switching between high and low drag can be modelled by switching estimated C_d between M2-A and M2-B if they are in different pointing states, or by assuming that the high-drag spacecraft has 2.1-2.5 times the drag of the low-drag spacecraft (obtained through experience).

A new GPS estimation data set of approximately 1-2 days duration is required whenever the spacecraft switches

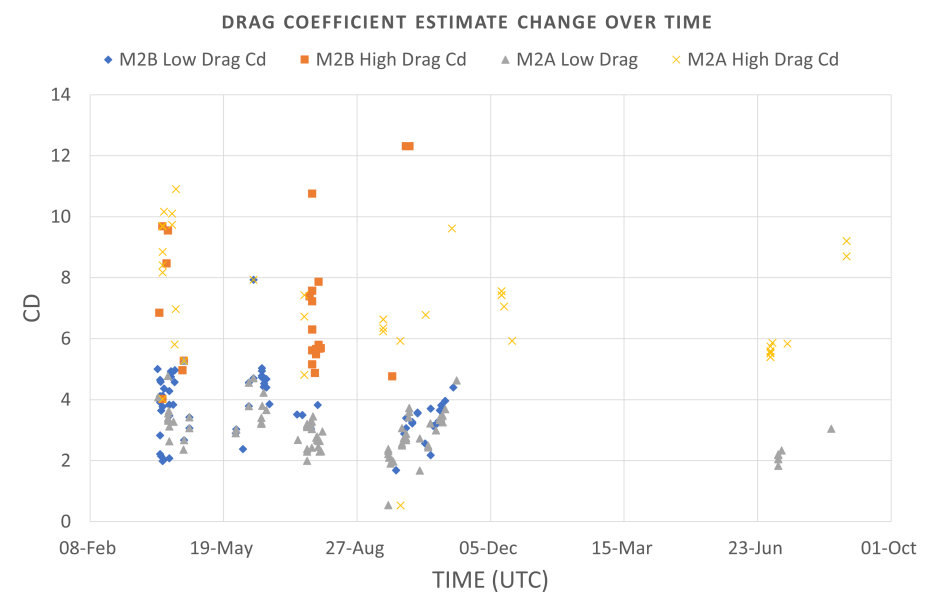

Fig. 3: variation of M2-A and M2-B drag coefficient estimate over time

between a high- or low-drag pointing attitude to achieve an accurate orbit state and C_d. The outcome is that after every attitude switch a significant delay is incurred before a good sufficiently trusted prediction of the future along-track separation is found. Furthermore, the concept of operations for the constellation dictates that only one spacecraft from the M2-A and M2-B pair shall be communicated on any given pass over the ground station, with only six passes in total available each day. The process becomes more complex in the event of an anomaly that causes a spacecraft to reset, which places the satellite in a slow tumble after it comes back online. When trying to fly the spacecraft in close proximity ($\leq$ 5km), these operational constraints present a logistical challenge to plan and execute the desired manoeuvre while ensuring that the spacecraft will remain sufficiently separated in the event of an anomaly.

Figure 4 shows the results of the close approach formation flying experiment conducted to support the "Sprint Advanced Concept Training 22-2" event in April 2022 [7]. The timing of the attitude changes was carefully orchestrated to provide the close approach ($<$ 2 km) during the 24-hour vulnerability window for the event. A key decision point for the operations team was on the 11^{th} April 2022, when M2-A was switched from high drag to low drag, allowing the formation to maintain a constant along-track separation of 1.5km-2km. The manoeuvre required ground station passes that aligned with the turning point of the measured GPS (yellow line) in Fig. 4 and required a significant amount of human-in-the-loop operation to ensure that the spacecraft would approach safely without drifting into each other.

The success of the close-proximity formation flying demonstration during SACT 22-2 is contrasted against the 23-2 event in July 2023 Fig. 5. The intended mission profile was to establish a fixed formation approximately 10km in separation, before crossing the spacecraft during the SACT event in the week of 12^{th} July. 2023 An overshoot in the approach the week prior required a correction to push the spacecraft apart, before performing the crossover manoeuvre. A minor geomagnetic storm on the 7^{th} July increased the uncertainty in the predicted atmospheric density for the propagation of M2-A and the TLE for M2-B , leading to mismodelling of the cross-over manoeuvre. The sensitivity of the current manoeuvre modelling approach to fluctuations and uncertainty in the atmospheric density is a major drawback with the current modelling approach.

2.2 Proposed Autonomous Closed-Loop Formation Control Approach

A simple and robust closed-loop autonomous control system is desired to better support the differential aerodynamic drag and formation flying tasks in support of the mission objectives of the space-based maritime / space surveillance mission and allow for a less intense workload when providing challenging SDA targets within SACT events. The approach shall:

1. Occupy a small footprint on the low SWaP (size, weight, and power) flight computers that shall not degrade the

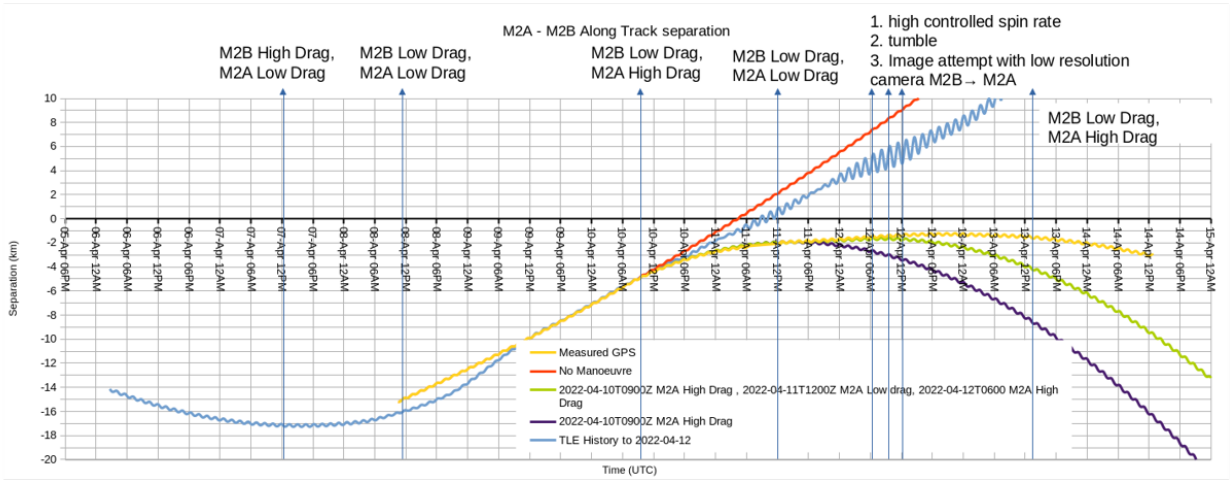

Fig. 4: Along-track separation distance of the M2-A and M2-B spacecraft during the SACT-22-2 event, taken from [7]

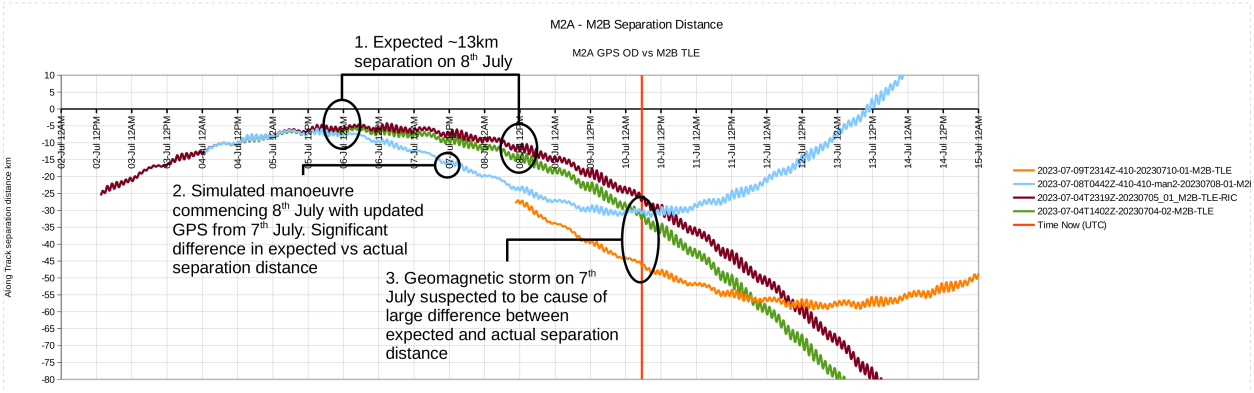

Fig. 5: Effect of atmospheric density uncertainty due to a G1 geomagnetic storm on 7th July 2023. Predicted (blue) vs actual manoeuvre profile for the M2-A and M2-B spacecraft during the SACT-23-3 event

performance of main mission activities

   (a) Minimise the size of the software change for upload to the spacecraft
   (b) Minimise the computational load/complexity when in operation
   (c) Minimise the power and heat requirements when in operation

2. Be reliable and robust to uncertainties in spacecraft attitude, relative position, C_d, atmospheric density prediction, and space weather events
3. Be reliable and robust to spacecraft anomalies
4. Not require a large amount of data exchange between the M2-A and M2-B spacecraft
5. Not require one satellite to autonomously task or control the other
6. Work when one of the spacecraft is offline or resets
7. Be easily tested and verified in ground tests on the flatsat hardware.

Control algorithms for differential aerodynamic formation control in the literature are typically developed from Clohessy-Wilshire-Hill (C-W-H) equations [11]. While C-W-H methods have enjoyed success for platforms with active propulsion, their ability to perform for differential atmospheric drag is less well established. For our specific requirements above, the C-W-H equations require a good state estimate, assume a known/constant C_d and a predictable current and future estimate for atmospheric drag. The C-W-H methods additionally require the spacecraft to communicate with each other to coordinate when and where changes in attitude/drag state shall occur.

As discussed above in Section 2.1 , experience has shown that 1-2days of GPS data are required in a fixed attitude to derive a reliable state and an estimate of C_d . The computational load to perform the batch least squares processing also exceeds the available computing resources for a process designed to support a main mission payload. The ability to test the approach on the ground is also limited. For these reasons, the C-W-H based methods are not selected for implementation. Likewise, machine learning approaches [12] that could potentially leverage the NVIDIA Jetson TX2 onboard the M2 spacecraft are not explored, as the power and thermal requirements for operation of this payload will exceed the resource allocation available for formation control.

The approach proposed here instead seeks to perform intersatellite ranging using the OpenLST UHF radio system on-board the spacecraft. The concept involves one spacecraft in the formation assuming a fixed 45° attitude, half way between high and low drag, throughout the manoeuvre. This provides the controlled spacecraft with the ability to achieve either a negative or positive drag differential without requiring any communication or coordination with the leader. The goal of the control algorithm is to provide a simple set of instructions to inform the chaser whether it should assume a high or low drag attitude based on the difference between the current range and the relative range of the spacecraft. A simple rate limiter based on the "distance to go" is applied to control the rate of change of spacecraft separation. Range-rate b (km/day) is calculated through a linear fit to average range measurements $\overline{R}$ (km) taken 6 times per day. Each average range measurement is calculated as a simple average of 30 range measurements taken at 10s intervals to reduce the effect of noise in the measurement. The control algorithm calculates a maximum allowable range rate b_{max} based on the difference between $\overline{R}$, a target separation range (R_{target}) and scaled by a factor (F) to avoid overshoots (Eqn. 1). S is a switch set by the satellite operators to identify whether the satellite performing autonomous control leads or lags in formation.

$$b_{max} = S\frac{(R_{target} - \overline{R})}{F} \tag{1}$$

$$C_d = \begin{cases} C_d^{min}, & \text{If } 0.5 < b \geq b_{max} \\ C_d^{max}, & \text{If } 0.5 < b \leq b_{max} \\ C_d^{min} + \frac{1}{3}(C_d^{max} - C_d^{min}), & \text{If } 0.5 > b \geq b_{max} \\ C_d^{max} - \frac{1}{3}(C_d^{max} - C_d^{min}), & \text{If } 0.5 > b \leq b_{max} \end{cases} \tag{2}$$

$$S = \begin{cases} 1, & \text{If control satellite leads} \\ -1, & \text{If control satellite lags} \end{cases} \tag{3}$$

If the measured range rate b exceeds b_{max}, then the spacecraft switches from a high drag attitude to a low drag attitude (Eqn 2). As $(R_{target} - \overline{R}) \to 0$, $b_{max} \to 0$ in Eqn 1 and the formation should settle to a stable oscillation around R_{target}, with the control satellite updating its attitude every 4 hours.

Robustness and reliability are added to the control scheme via uploading an ephemeris regularly to the control satellite for the target satellite (TLE or higher-fidelity ephemeris). In the event that the target satellite resets or the inter-satellite ranging system fails, the control satellite can perform pseudorange estimates from its GPS system referenced against the target satellite ephemeris. The target/non-controlled satellite will be tumbling after a reset, however the average drag coefficient of the tumbling spacecraft will be close to the 45° fixed attitude assumed by the controller. If the control satellite resets and cannot perform the autonomous formation control, then the non-controlled satellite can be commanded to become the new control satellite during the next pass over the ground station. The simple range-rate-based control approach can also respond to fluctuations in the atmospheric density without the need for onboard atmosphere modelling, as the method does not require any state estimation.

2.3 Inter-satellite Ranging using a UHF Radio

The M2 spacecraft feature an in-house UHF radio system developed on Planet's open source OpenLST design. OpenLST has been used on over 200 of Planet's Dove satellites and the design has extensive flight heritage. The datasheet for the radio provide the following specifications:

- Transmit Power: 1W
- Frequency: 450MHz
- Receiver Sensitivity: -112dBm
- Ranging Performance: 1km RMS

The stated ranging performance of 1km RMS can be improved through careful characterisation of the processing delays. The system clock is 27 MHz, which equates to a 37 ns period, corresponding to 11 m/period. The oscillator used (Fox924) has a drift of 2.3 ppm + ageing of 1 ppm per year, but for now let us just consider the 2.3 ppm. This is equivalent to $\pm$ 62 cycles/second, or a potential cycle slip every 16 ms. The transmitter (the ranging spacecraft) starts a stopwatch from the moment the packet is sent by the radio. Upon receiving a response, the timer is stopped. The time is quantised to the clock period, which introduces an uncertainty of the clock cycle time plus potential clock slips due to the clock drift. On a 100 km ranging, the round trip time of flight of the signal would be 2*100km/c = 670 μs. This is 4% of a potential cycle slip, adding 1.5 ns of uncertainty to the measurement. Thus, assuming that all the delays in the second spacecraft are deterministic and quantifiable, we should have an uncertainty of 37 + 1.5ns = 38.5 ns or 38.5 ns * c = 11.5 m.

This is also under the assumption that zero crossings in the packet on the RF channel can be detected with a higher time resolution than the system clock period. Quantifiable and known delays here also include packet length and emission time, packet detection, and decoding time. In reality, the second spacecraft receives the packet and sends a ranging response back. This involves: detecting the packet, decoding the packet, decision making in the processor, building response, and transmitting response. The first two are deterministic and quantifiable as the length of the packet and location of the header are known; however, the processing time in the micro-processor is more uncertain. While no operating system is running, we are affected by:

1. Interrupt priorities: RF or DMA interrupts can override timer interrupts. This means that potentially extra code is executed taking 100's of clock cycles. However, only RF and DMA can override the timer. Initially, upon reception, the RF interrupt can start the timer (stopwatch). If we wait a deterministic amount before sending a response, such that all interrupts have finished, this uncertainty here is negligible. False detections of packets and such can reset the timer and render the measurement invalid
2. The current instruction has to finish. In worst case this is 11 cycles = 370 ns (110 m) but more typically it is 4 cycles or 111 ns (33 m)

3. The time to switch into the interrupt handling has some variance to it.

It is worth noting that all of the above uncertainties increase the round-trip time and therefore the distance. Through performing repeated measurements and taking the ones with the lowest values, we should be able to get the uncertainty of the processing in the second spacecraft down to 111 ns or 33 m. This results in a total uncertainty of less than 45 m at a separation distance of 100 km. The range error decreases with proximity to the spacecraft (Tables 1 and 2). The analysis here assumes a normally distributed range error with a RMS of 45 m.

The feasibility of the intersatellite range approach was demonstrated on 8^{th} December 2022, when an intersatellite relay test was performed in which M2-B relayed a signal received from M2-A down to the UNSW Canberra Space ground station in Yass, near Canberra. Testing of the time-of-flight range with the radios was not performed during the test; however, the successful receipt and retransmission of packets from M2-A by M2-B confirms that a link can be established from a separation distance of at least 100 km.

Table 1: Uncertainty due to clock errors

Range [m]	Round trip time [s]	% of a slip	Extra delay [s]	Total uncertainty [s]	Total uncertainty [m]
1.00E+03	6.67E-06	0.000414	15.33E-12	37.05E-09	11.12
10.00E+03	66.67E-06	0.00414	153.33E-12	37.19E-09	11.16
100.00E+03	666.67E-06	0.0414	1.53E-09	38.57E-09	11.57
1.00E+06	6.67E-03	0.414	15.33E-09	52.37E-09	15.71

Table 2: Total uncertainty [m]

Range [m]/bandwidth [Hz]	**1.50E+04**	**3.50E+04**	**1.00E+05**	**5.00E+05**
1000	12.78	12.21	11.76	11.40
10,000	27.80	22.06	17.60	14.04
100,000	178.04	120.55	76.04	40.40
1,000,000	1.68	1.11E+03	660.44	304.04

3. RESULTS

The proposed autonomous control approach is tested using simulations initialised with states derived from GPS data collected during previous close proximity formation flying attempts during the SACT-22-2 event in April 2022 and recent experiments studying the feasibility of flying in formation with M2-B using TLE-based ephemeris, beginning with the SACT 23-3 event in July 2023.

3.1 SACT-22-2 12^{th} - 15^{th} April 2022

The SACT-22-2 event demonstrated the ability for differential aerodynamic drag to bring the M2-A and M2-B satellites from over 50km separation distance to within 2km of each other Fig . 4. For the purposes of this study, the accuracy of the predicted manoeuvre with the measured GPS positions of the spacecraft validates the GMAT modelling approach and provides a framework to study the proposed autonomous formation control approach. The estimated state for M2-A and M2-B from GPS data collected over 1^{st} - 4^{th} April 2022 is used to initialise the simulation. Two scenarios are simulated:

1. M2-A is tasked with approaching and holding a 2 km separation distance with M2-B from its initial 20km separation, replicating the manoeuvre performed via the human-in-the-loop process
2. M2-A is tasked with approaching and holding a 100km separation distance from M2-B to study the stability of the control algorithm over larger distancess

A neutral 45° attitude is applied to M2-B at its epoch, derived from the average of the C_d^{max} and C_d^{min} values obtained from the orbit determination process for M2-B during the SACT-22-2 event. The C_d values used for the simulation

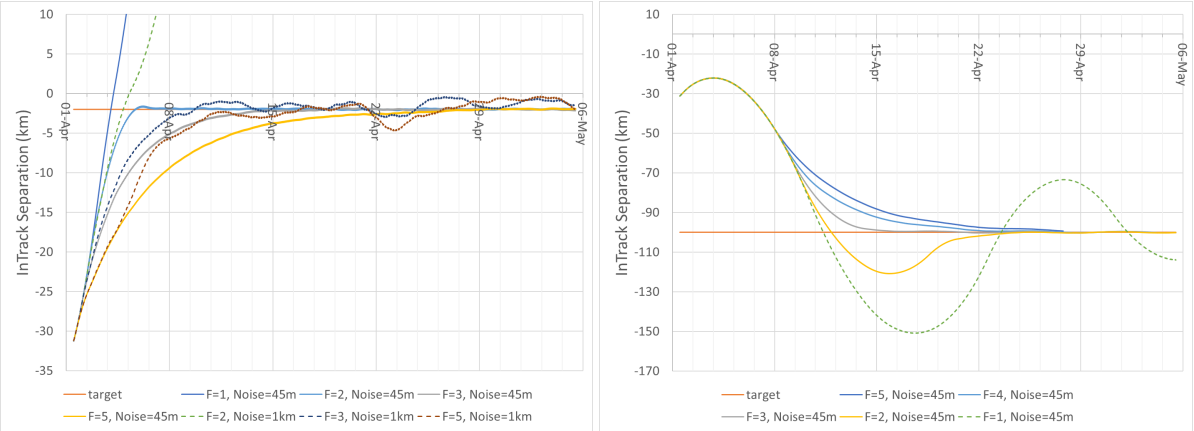

(a) 2km target separation

(b) 100km target separation

Fig. 6: Effect of scale factor F and noise for a 2km and 100km target separation during the SACT-22-2 event

are shown in Table 3 and assumed identical for both spacecraft. The performance of the control algorithm is studied for the 2 km and 100 km cases above for different values of F (Eqn. 1). The effect of inter-satellite range uncertainty derived in Table 2 on the stability of the control scheme are also investigated. The results for the 2 km separation case are shown in Fig. 6a. Decreasing F reduces manoeuvre time, however, the F = 1 case overshoots the target separation distance sufficiently to cause the spacecraft leader/chaser order to switch, resulting in the controller forcing the spacecraft to diverge. A value of $F = 3$ provides a good balance between performance and stability, providing the desired 2 km target separation distance by 15^{th} April. The close approach manoeuvre performed during the SACT-22-2 event achieved the 2km separation distance on 11^{th} April and nominally outperforms the manoeuvre simulated here, however this is an expected result as both spacecraft were commanded into their maximum and minimum drag configuration and therefore had a larger drag differential force compared with fixing M2-B at a neutral 45° angle. Increasing the uncertainty of the range from 45 m to 1 km caused the $F = 2$ case to overshoot and diverge when the leader/chaser order is switched. The $F = 3$ and $F = 5$ cases experience oscillations around the target 2 km separation distance. The effect of F is more pronounced for the 100 km case, Fig. 6b, with the $F = 1$ and $F = 2$ showing large overshoots before converging to the target 100 km separation target.

Table 3: C_d bounds estimated for the SACT-22-2 event

Cd_min	**Cd_min+30%**	**Cd_neutral** (M2-B)	**Cd_max - 30%**	**Cd_max**
4	5.67	6.5	7.33	9

3.2 Pseudo-Ranging with M2-B Two-Line Elements

Figure 7 plots the difference for in-track, radial and cross-track error between the spacetrack TLE history from 2023-08-23 to 2023-08-26 for M2-A GPS data. The residuals from the batch least-squares orbit determination fit are also included to highlight the difference in uncertainty for relative range measurements between the high fidelity fitted and TLE orbits. The TLE difference has a median difference of 524 m compared to the residual mean for the orbit determination of 20 m. Figure 7 shows that ranging against the TLE introduces significant noise and uncertainty compared to the inter-satellite RF ranging approach.

The concept proposed in Sec.2.2 is to periodically upload the M2-B TLE to the M2-A spacecraft, which can be used to perform a pseudo-range measurement using the GPS onboard M2-A. The effectiveness of the TLE-based formation flying approach has been examined using an ephemeris constructed from multiple TLEs ranging from 2023-08-10T to 2023-08-30T for M2-B with the control scheme used in Sec. 3.1 applied to M2-A (Fig. 8a). The M2-A state was obtained from an orbit determination process using M2-A GPS data ranging from 2023-08-10T to 2023-08-14T, corresponding to a low drag pointing state, giving $C_d^{min} = 2.99$. High drag C_d^{max} was estimated as $2.5 * C_d min = 7.5$ and a target separation distance of 715 km applied. The results show that formation flying to the TLE presents a greater challenge than the intersatellite ranging approach. The C_d plot in Fig. 8a shows a high frequency of switching between

Fig. 7: TLE and Batch Least Squares (BLS) orbit determination residuals measured against GPS data for the M2-A spacecraft

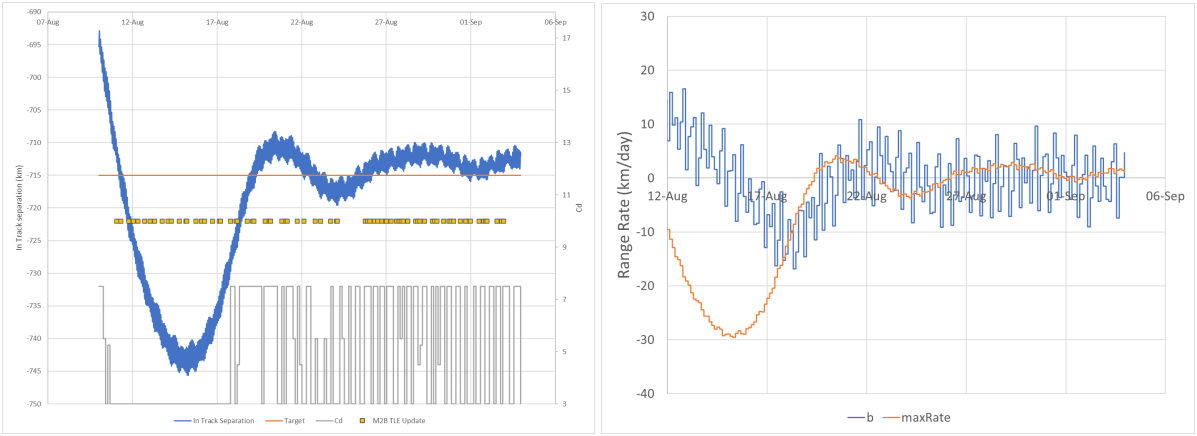

(a) Range and C_d

(b) Range rate

Fig. 8: Autonomous formation flying simulation for M2-A against the M2-B TLE, August 2023

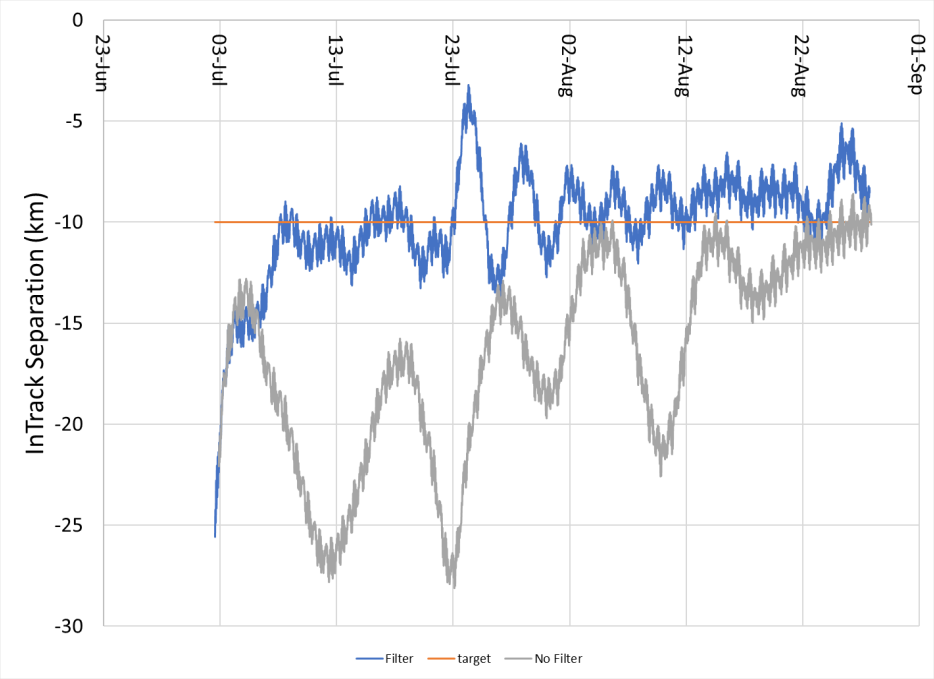

Fig. 9: Simple filtering for TLE-based range estimation

high and low drag as the controller attempts to stabilise on the 715 km separation target. The reason for the under- and overshoots is the periodicity for the range derived from the simulated orbit and the lower fidelity mean TLE set. Figure 8b highlights the problem, where the noise in the computed range is amplifed when taking the range rate using the simple differencing approach proposed, resulting in b causing C_d to switch rapidly in Eqn. 2

3.3 SACT-23-2 10^{th} - 14^{th} July 2023

A modification to the TLE-based ranging approach is applied to a case study for the SACT-23-2 event in July 2023, where the intended close approach was unable to be performed with the spacecraft due to mis-modelling of the relative trajectories arising from the minor geomagnetic storm on 7th July (Fig. 5). M2-B had reached its end of life prior to this experimental window and no GPS data was available, requiring the formation flying to be performed against the TLE history for M2-B. The case study is used to assess whether the proposed TLE-based ranging approach would have the ability to autonomously respond to the 7^{th} July space weather event to keep the spacecraft at a target separation range of 10 km. A simple filter was employed to help smooth the oscillations present with the TLE-based ranging approach while maintaining an acceptably small computational overhead, defined in Eqn 4 .

$$y+ = \alpha * (x - y) \tag{4}$$

where $\alpha = \Delta t/\tau, \Delta = 300s, \tau = 1day$

Figure 9 shows an improvement in the ability to hold the 10 km target separation range over the nonfiltered solution, however significant oscillations remain around the target point. Figure 10 shows that the filter has been effective in reducing the noise in the range rate estimation and b_{max} , however a more complex filter and smoothing algorithm is clearly required if a stable 10 km separation distance is desired. Tuning α, F , and the propagation time between measurements had a strong impact on the ability to hold the commanded 10 km separation distance and did not hold for simualtions performed under different initial conditions. Future work will develop a higher-order filter suitable for the satellite platform to assist with TLE-based formation flying. An initial study employing a 2^{nd} order Butterworth filter with forward and backward smoothing to TLE histories of M2-A and M2-B during a manual formation stabilisation manoeuvre show promise. Figure 11 shows that the range rate obtained from the filtering would result in only 4 changes in C_d from Eqn2 when b intersects the b_{max} line.

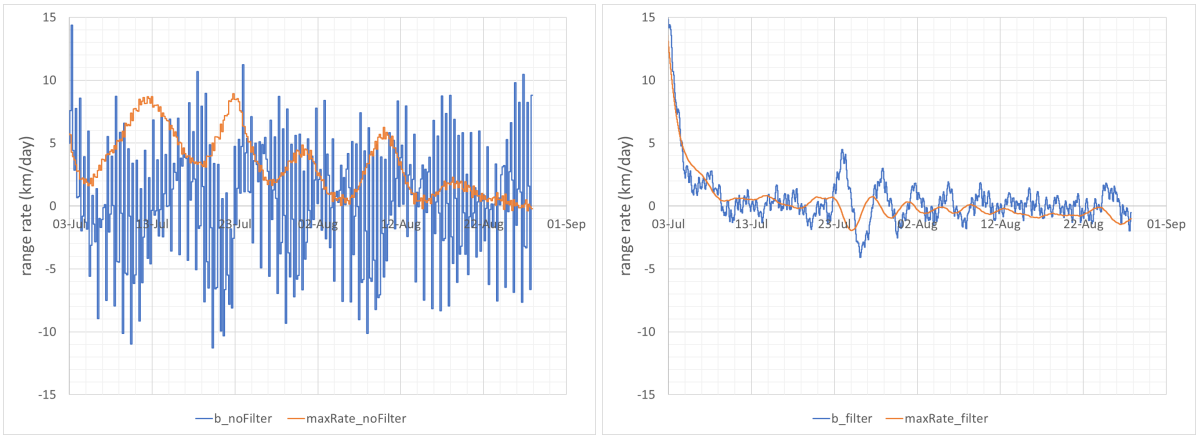

(a) No filter (b) Filter

Fig. 10: The effect of applying a simple low pass filter to TLE-derived range rate for the SACT-23-3 case study

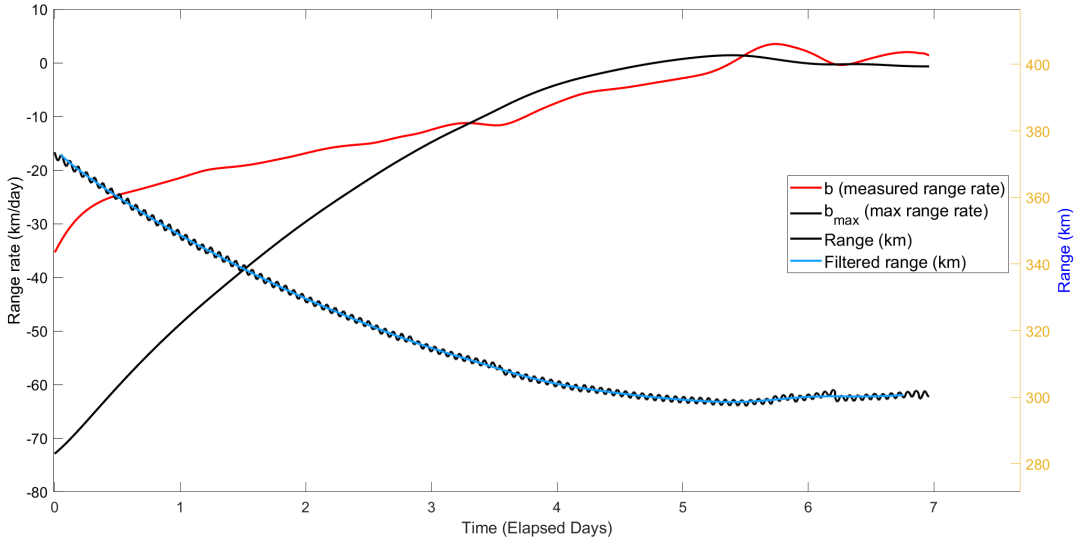

Fig. 11: 2^{nd} order Butterworth filter applied to TLE data for M2-A and M2-B during a formation stabilisation test manoeuvre

4. ACKNOWLEDGEMENTS

This work was funded by the Royal Australian Air Force and the Asian Office of Research and Development (AOARD).

[1] Dave Guglielmo and Riccardo Bevilacqua. Propellant-less atmospheric differential drag leo spacecraft (paddles) mission. In *Proceedings of the 2014 SmallSat Conference*. Digital Commons Berkeley, CA, 2014.

[2] Christopher S Ruf, Clara Chew, Timothy Lang, Mary G Morris, Kyle Nave, Aaron Ridley, and Rajeswari Balasubramaniam. A new paradigm in earth environmental monitoring with the cygnss small satellite constellation. *Scientific reports*, 8(1):8782–13, 2018.

[3] David Pérez and Riccardo Bevilacqua. Lyapunov-based adaptive feedback for spacecraft planar relative maneuvering via differential drag. *Journal of Guidance, Control, and Dynamics*, 37(5):1678–1684, 2014.

[4] M Horsley, S Nikolaev, and A Pertica. Small satellite rendezvous using differential lift and drag. *Journal of Guidance, Control, and Dynamics*, 36(2):445–453, 2013.

[5] Constantin Traub, Francesco Romano, Tilman Binder, A Boxberger, GH Herdrich, S Fasoulas, PCE Roberts, Katharine Smith, Steve Edmondson, Sarah Haigh, et al. On the exploitation of differential aerodynamic lift and drag as a means to control satellite formation flight. *CEAS Space Journal*, 12(1):15–32, 2020.

[6] Cyrus Foster, James Mason, Vivek Vittaldev, Lawrence Leung, Vincent Beukelaers, Leon Stepan, and Rob Zimmerman. Constellation Phasing with Differential Drag on Planet Labs Satellites. *Journal of Spacecraft and Rockets*, 55(2):1–11, 2017.

[7] M. Brown, R. Boyce, A. Lambert, E. Peters, S. Gehly, S. Boland, R. Jeffreson, A. Kremor, T. Bateman, C. Capon, B. Smith, G. Bowden, L. Glina, L. Qiao, S. Balage, K. Gupta, R. Purwanto, T. Bessell, T. Reddell, J. Bennett, M. Lachut, and T. McLaughlin. Formation Flying and Change Detection for the UNSW Canberra Space 'M2' Low Earth Orbit Formation Flying CubeSat Mission. In *Advanced Maui Optical and Space Surveillance Technologies Conference*, page 18, September 2022.

[8] Melrose Brown, Brenton Smith, Christopher Capon, Rasit Abay, Manuel Cegarra Polo, Steve Gehly, George Bowden, Courtney Bright, Andrew Lambert, and Russell Boyce. Ssa experiments for the australian m2 formation flying cubesat mission. 2020.

[9] Steven P Hughes. General mission analysis tool (gmat). Technical report, 2016.

[10] David A Vallado and TS Kelso. Earth orientation parameter and space weather data for flight operations. In *23rd AAS/AIAA Space Flight Mechanics Meeting, Kauai, HI*, pages 2679–2698, 2013.

[11] Brenton Smith, Russell Boyce, Laurie Brown, and Matthew Garratt. Investigation into the practicability of differential lift-based spacecraft rendezvous. *Journal of Guidance, Control, and Dynamics*, 40(10):2682–2689, 2017.

[12] Brenton Smith, Rasit Abay, Joshua Abbey, Sudantha Balage, Melrose Brown, and Russell Boyce. Propulsionless planar phasing of multiple satellites using deep reinforcement learning. *Advances in Space Research*, 67(11):3667–3682, 2021.